SEASONAL INVESTIGATION ON PREDICTION ACCURACY OF ATMOSPHERIC TURBULENCE STRENGTH WITH A NEW MODEL AT PUNALKULAM, TAMIL NADU

© 2016 **A. Arockia Bazil Raj**[*], Associate Professor; **J. P. Lancelot**[**], Engineer

[*]Laser Communication Laboratory, Kings College of Engineering, Punalkulam-613 303, Thanjavur, Tamil Nadu, India
[**]Photonics Division, Indian Institute of Astrophysics, Bangalore-560 034, Karnataka, India

E-mail: brazilraj.a@gmail.com

Atmospheric parameters strongly affect the performance of Free Space Optical Communication system when the optical wave is propagating through the inhomogeneous turbulence transmission medium. Developing models to get an accurate prediction of turbulence strength (C_n^2) according to meteorological parameters becomes significant to understand the behavior of channel in different seasons. A dedicated Free Space Optics link for the range of 0.5 km at an altitude of 15.25 m is established and explained. The power level and beam centroid information of the received signal with meteorological parameters at the same time are continuously measured using the optoelectronic assembly and developed weather station respectively and stored in a data logging computer. The existing models selected, based on exhibiting relatively less prediction error, for comparative analysis are briefed. Measured meteorological parameters (as input Factors) and C_n^2 (as response Factor) of size [2000×4] are used for linear regression analysis and to design the empirical models more suitable at the test field. Along with the model formulation methodologies, contribution of input factors individual and combined effects on the response surface and coefficient of determination (R^2) estimated using Analysis of Variable tools are presented. Model equation-V ($R^2 = 98.93\%$) is finalized for predicting C_n^2. In addition, the prediction accuracy of the proposed and selected models for different seasons in one year period are investigated and validated in terms of Sum of Absolute Error (SAE). The average SAE of 0.000641×10^{-9} $m^{-2/3}$ for C_n^2 is achieved using the new model in longer range dynamic of meteorological parameters during different local seasons.

Keywords: *meteorological data, regressive model, model equation-V, scintillation, beam wandering, and optical turbulence strength.*

OCIS codes: 010.1330, 120.3940, 200.2605, 330.7326, 290.5930

Submitted 03.07.2014

1. Introduction

Free Space Optical Communication (FSOC) is a potentially high capacity and cost effective technique that receives growing attention and commercial interest. Free Space Optics (FSO) is an age long technology that entails the transmission of information laden optical radiation through the atmosphere from one point to other. FSOC through the atmosphere is important to commercial and defense applications. Two of these applications are last-mile links and mobile battlefield networks. The advantages of optical communications through the atmosphere over radio communications include increased security, unlicensed and large bandwidth. Packet switching is also widely employed in optical communications through the atmospheric access network [1–3]. The limiting factor in FSOC is intensity noise due to the fluctuations of the atmospheric parameters, so called capacity limiting factors, which depends on the local meteorological conditions that cause the propagating laser beam to be deflected and/or scattered [4–7]. The scattering coefficient is defined as the ratio of original light intensity (scene irradiance) to attenuated scene intensity (irradiance) [8–10]. While these deviations are small locally, the effects accumulate over the propagation

path and can lead to scintillation, beam wandering and wave front distortion that varies on timescales typically in the order of a millisecond or longer [3, 8, 10–13] which reduce the overall system reliability. Hence, it is reasonable that, in a real FSOC environment, optical channels will appear to have randomly time varying characteristics which are difficult to predict/simulate. Different weather conditions including dust, eddies of air of various size and velocity, fog and smoke are the sources that could potentially disrupt the FSOC by attenuating (scintillating) the input optical signal to the receiving side [10, 14–16].

The disturbance of atmospheric turbulence varies greatly with location and time and its strength is usually greater near ground and falls-off exponentially with increasing altitude due to wind shear. As a result of the exponential distribution, the effects of turbulence are much less severing in near-vertical path than in horizontal propagation path of comparable length [16, 17]. In this point of view, real time experimental study on the turbulence strength (C_n^2) as the function of meteorological parameters are important to understand the channel effects on the propagating optical beam to characterize the FSO channel that the maximum data rate the system could be able to operate at the test field. The Earth Observation Satellite (EOS) view of the experimentation field location representing the transmitter and receiver established for this study is shown in Fig. 1. The AC plant, Mechanical workshop, Civil engineering block, playground and Agriculture land are the terrain disturbance sources in addition to the atmospheric changes to the optical pathway. The transmitter lab is located on a tower (lat. 10°38′46.7334″ and long. 79°3′12.0774″) while the receiver is built on the rooftop of the existing Information Technology (IT) block (lat. 10°38′52.8468″ and long. 79°2′56.6268″) of Kings College of Engineering, Punalkulam, Tamil Nadu, India as in Fig. 1. Meteorological sensors, as described in paper [18], are deployed close to transmitter, receiver and at the midway of the optical link. The wireless data logging hardware circuits are connected with the receiver unit and the measured weather data are recorded in the computer. Dozen of models are available for predicting the atmospheric turbulence strength. The sufficient criticism on the existing models and the root-cause for/of the new models can be found in several recent publications including [6, 10–12, 15, 19]. These models are explicitly experimentally

Fig. 1. Bird view (EOS) of optical propagation path for atmospheric C_n^2 field data measurement. The receiver system is located on the building at the left (*1*) and the transmitter system is located on the tower at the right (*2*).

investigated to test the robustness at our test field. The experimental outcomes clearly demonstrate that in spite of significant number of investigations the prediction results of these models contradict among themselves when applied at our atmosphere and exhibit less correlation with the measurement data acquired for several days in different seasons. Development of the accurate and locally valid model to predict the C_n^2 according to local weather data becomes interesting and important, which is the main contribution in this paper, to design a suitable mitigation technique to improve the overall performance of the FSOC system [3, 20].

The rest of the paper is organized as follows: section 2 presents the background and related works, section 3 describes the transmitter and receiver experimental setups and optoelectronic assembly, section 4 reviews some of the existing models selected for the comparative analysis, section 5 demonstrates the development and validation of proposed models of C_n^2, section 6 discusses the experimental results and data analysis and section 7 draws some conclusions.

2. Background and Related Works

In the last few years, a lot of in situ field measurements related to the modeling of C_n^2 have been remarkably carried out and can be found in the literature. Some of the closely related works are briefed below: W. Ni et al. have developed a RF-FSO test link and studied the atmospheric turbulence effects on these two links. The turbulence strength is estimated using the Rytov variance and Angle-of-Arrival (AoA) methods with the link

range of 300 m between two buildings in Hamamatsu Photonics K.K [4]. Vinicius N.H. Silva et al. have used the beam wandering based technique (triangulation-like) to estimate the C_n^2 using 21 cm optical link set-up. It is similar to the Optoelectronic Position Detector (OPD) where the radial displacement is the principal component. The optical beam tracking and simulation results for various displacements are discussed [5]. Arnold Tunick has briefed the geographical and terrain location of the experimental setup. The method of environmental and C_n^2 data acquisition and analysis are given. The data correlation and curve fit equations are discussed. The influence of wind vector is briefed [7]. Jaume Recolons et al. have discussed various theoretical models on Root Mean Square (RMS) of centroid displacement, beam wander variance and spot size, hot spot displacement, beam parameters, profile of untracked and tracked beam, beam radius, mean irradiance profile and scintillation index. The simulation results are discussed [9]. Troy T. Leclerc et al. have described the optical and meteorological equipments used in the experimental setup. Macro-meteorological models (as a function of weather data) developed/modified by Bendersky, Kopeika, and Blaunstein (BKB model) are given. The BKB model utilized the −4/3 height scaling power law introduced by Walters and Kunkel and the experimental data corresponding to various days are presented. The optical path distance of 65 m is used [11]. D. Sadot et al. have described various methods of C_n^2 prediction. The experimental setup and location (Tx and Rx) information are detailed. A regression model is presented and experimental data are analyzed. The predicted values are validated against the measurement data [12]. Yitzhak Yitzhaky et al. presented the macro-meteorological model for predicting C_n^2 and aerosol modulation transfer function. The restorations of atmospherically blurred images are the principal components. Image restoration and C_n^2 estimation results are reported in paper [14]. Sergey Bendersky et al. have clearly explained the C_n^2 experimental site, instrumentation and measurement data. A detailed analysis of Monin-Obuhkov similarity models is given. The statistical data corresponding to the deviations among these models and against the measurement data are explained [15]. Arun K. Majumdar et al. have briefed the theoretical concepts of atmospheric turbulence effects. Various atmospheric turbulence models (as a function of altitude) for estimating turbulence strength, coherence strength, isoplantic angle, Rytov variance and greenwood frequency are explained. Experimental procedure and data collected on different days are discussed [17]. Arnold Tunick has described the optoelectronics experimental setup configuration for the optical turbulence measurement over a 2.33 km free-space laser path. The Rytov variance approach is followed to measure the C_n^2 and the values are compared against the scintillometer data [21]. Steve Zamek et al. described the methods of estimating AoA variance and spatial and temporal correlation properties. The C_n^2 is estimated from the blurred image and the results are presented [22].

3. Experimental setup at Punalkulam, Tamil Nadu and Data Acquisition

Transmitter and receiver laboratories are established for the link range of 0.5 km at an altitude of 15.25 m at Punalkulam, Tamil Nadu, India exclusively for the studies on prediction of atmospheric attenuation, as described in paper [10], and C_n^2 according to local weather data. A semiconductor laser source, data generator (in FPGA), optical modulator and transmitting optics are the main optoelectronics devices at the transmitter. The transmitting optics is used to expand the incident beam of diameter 3 to 9 mm to reduce the beam divergence at the aperture of the receiving optics (telescope). The receiver laboratory consists of telescope, Narrow Band Interference Optical Filter (NBIOF), variable beam splitter, photodiode, OPD, Mono-Pulse Arithmetic Circuit (MPAC), optical power meter, automated Data Acquisition Card (DAC) Advantech ADAM 5000 series hardware and data logging computer (PC). The optoelectronics equipments are assembled such as to measure power fluctuation in milliwatt and beam displacement in volt as suggested in publications [23–25]. The telescope captures all the photons and concentrate them to the NBIOF which is used to permit only the 850 nm (center wavelength) optical beam as well as to block the other wavelengths.

The variable beam splitter divides the incident beam (output of the NBIOF) into two directions: reflecting and propagating beam. The reflected beam is made to fall on the OPD to measure the beam wandering information using the MPAC computations as described in papers [3, 20, 25]. The propagating beam is made to fall

on the photodiode and its output is connected to the power meter. The schematic diagram of experimental setup is shown in Fig. 2 and all the optoelectronic devices are mounted on the vibration damped optical breadboards as shown in Fig. 3. A low cost and high accuracy integrated weather station is built with specialized sensors to continuously measure the wind speed (Ws), temperature (T), relative humidity (RH) and pressure (P) as described in paper [18].

The weather station is deployed at an altitude of 15.25 m near to the transmitter, receiver and at the mid-point (above civil block). The meteorological data were continuously acquired every second during different outdoor environmental conditions (local seasons) and the day-wise data are averaged over 5 min period. A separate Graphical User Interface (GUI) is developed using MATLAB environment [26] for automated data acquisition through RS232 communication port, data logging

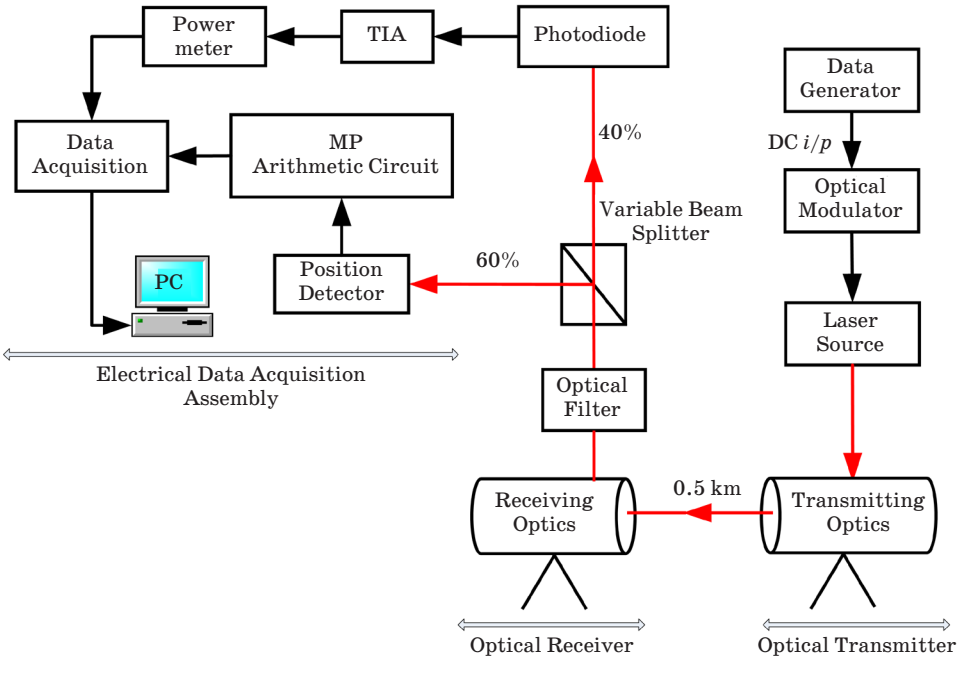

Fig. 2. Schematic diagram of Laser Communication Laboratory (LCL) experimental setup (optical transmitter and receiver) with electrical data acquisition assembly.

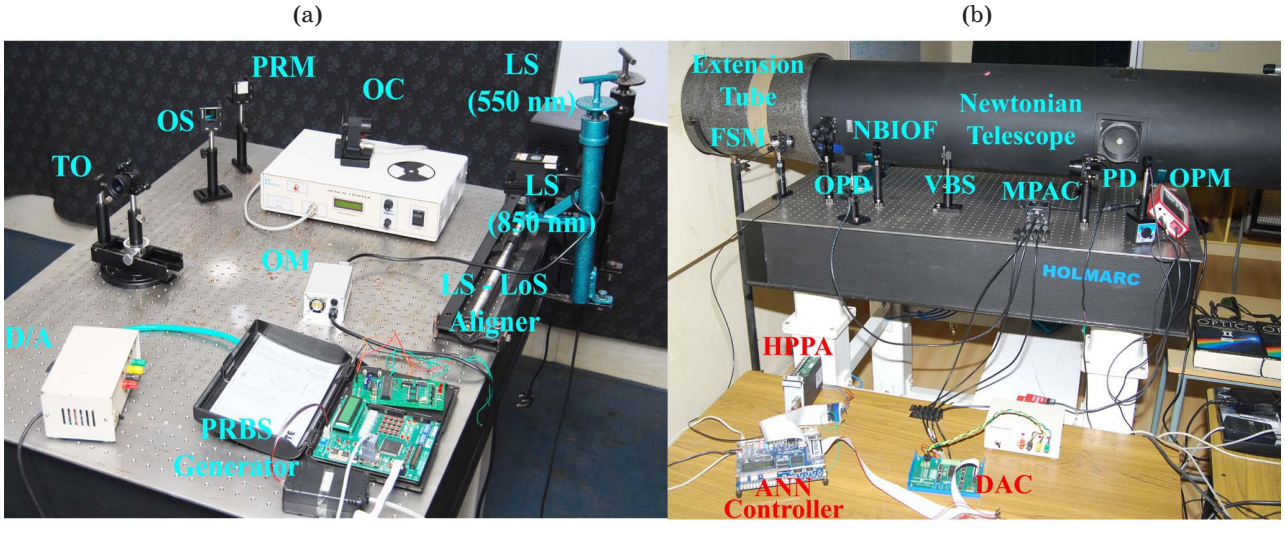

Fig. 3. Snapshot showing the optoelectronic components assembly on the vibration damped optical bread board (a) transmitter and (b) receiver.

Table 1. Experiment parameters of the optical link

Parameter		Value
Transmitter		
laser diode	peak wavelength, nm	850
	maximum optical power, mW	10
	beam size at aperture, mm	3
	beam divergence, mrad	3
	laser beam propagation model	plane
transmitting optical	diameter, mm	3:9
channel	range, km	0.5
	altitude, m	15.25
	surface roughness length, m	0.03
Receiver		
telescope	aperture, mm	330:9
	type	Newtonian
filter	type	NBIOF
	CWL, nm	850
optical collimator	collimation ratio	9:3
beam splitter	type	variable
	splitting range, %	0–100
OPD	error output, V	±10
	position sensitivity, mm	±2
	error computation	MPAC
photodetector	active area, mm^2	1
	half angle field of view, degree	±75
	spectral sensitivity, A/W	0.59
	rise and fall time, ns	5
power meter	thorlabs – PM100D, nm	400-1100

and on/off line computations. The main optoelectronics devices and their parameters are given in Table 1.

The necessary parameters are extracted from the measurement values and applied to the models to predict the C_n^2 in $m^{-2/3}$.

4. Review on existing models considered for comparative analysis

The optical radiation traveling through the atmospheric turbulent channel interacts with the molecular constituents of the atmosphere and causes some of the photons extinguished. This event ultimately results in power loss, temporal and spatial distortion that strongly depends on the local weather conditions/seasons [2, 3, 10–13, 15, 20, 27]. Although various wavelength independent/dependent models are available, the models exhibiting relatively less SAE are considered for the comparative analysis with the new models. The selected models are reviewed in this section with their backgrounds and limitations. The detailed descriptions of the selected models can be found in references. Most of the models found in literature predict the C_n^2 as a function of altitude and their prediction results greatly defer from the measurement data of horizontal path turbulence. Furthermore, some of the models are developed for specific locations like rocky terrain, Hufnagel-Valley (HV)-night time, Submarine Laser Communication (SLC)-day, Greenwood and Gurvich etc. The C_n^2 not only varies as a function of altitude, but also according to local meteorological conditions, geographic location, terrain type and time of day [10, 13, 17, 27]. Therefore, the models predicting the horizontal turbulence strength and exhibiting less SAE are only considered for the comparative analysis.

4.1. PAMELA model

According to PAMELA model, the turbulence fluctuation in the surface boundary layer is a function of altitude (*h*), local conditions (terrain type), geographical location, cloud cover, meteorological values (Ws, *T*, RH, *P*), latitude, longitude, number of day in year, Greenwich Mean Time (GMT), surface roughness length and local time of day [11]. The PAMELA model given in Eq. (1) provides C_n^2 estimation within the surface boundary layer and it accepts all the above parameters of test field as the inputs. The measured meteorological parameters [18] are given to the model to estimate the turbulence strength.

$$C_n^2 = 5.152\varphi_h \left(\frac{1}{\varphi_m - \varsigma}\right)^{0.33} \times \times \left(\frac{77.6\times10^{-6}P}{T^2}\right)^2 h^{-0.667}\left(\frac{-H}{C_\rho \rho u*}\right)^2, \quad (1)$$

where φ_h is temperature gradient, φ_m is wind shear estimated from the Ws, ζ is eddy dissipation rate, H is heat flux, C_ρ is specific heat, ρ is mass density and u_* is friction velocity. As can be seen

from Eq. (1), $C_n^2 \to \infty$ as Ws $\to 0$ [19, 27], therefore, the minimum Ws is bounded away from zero i.e 0.27 ms^{-1}.

4.2. Hufnagel-Valley model

Hufnagel-Valley model predicts the C_n^2 for inland sites and daytime viewing conditions since it permits variations in altitude, Ws and near ground turbulence levels. In this model, a sum of three exponential decay terms corresponding to a surface boundary layer, a strong layer caused by the high-altitude jet stream and a background tropopause layer are present [15] as in Eq. (2)

$$C_n^2(h) = A\exp(-h/100) + 5.94 \times \\ \times 10^{-53}(v/27)^2 h^{10}\exp(-h/1000) + 2.7 \times \\ \times 10^{-16}\exp(-h/1500), \quad (2)$$

where A is the nominal value $C_n^2(0)$ of C_n^2 in m$^{-2/3}$ at the ground and v is the Root Mean Square (RMS) Ws in ms^{-1}.

4.3. Beam Wandering model

The beam wander effect is related to the displacement of the instantaneous center of the receiving beam: the point of maximum irradiance of a traveling wave over the OPD plane. It is well known that this phenomenon is caused by the large-scale inhomogeneities due to their refractive effects [5, 9]. In the 2D Cartesian or polar coordinate (x, y or r, θ) receiver plane, the stochastic polar variable γ_c (radial displacement) of the beam center is computed by coordination transformation as [5]

$$\gamma_c = \sqrt{x_c^2 + y_c^2}, \quad (3)$$

where x_c and y_c are the Cartesian coordinate of the center of the Gaussian light spot on OPD and used to track the beam wander with respect to origin (0,0) mm as detailed in [3, 20, 25]. The beam wander can be statistically characterized by the variance of γ_c and related with the atmospheric turbulence strength using the geometrical optics approximation as [5, 7]

$$C_n^2 = \frac{\left\langle \gamma_c^2 \right\rangle}{2.42R^3W^{-1/3}}, \quad (4)$$

where W is beam waist (width) of the Gaussian beam in mm and R is length of the optical link in km.

4.4. Polynomial regression

This model is developed to obtain the best estimation of C_n^2 according to the macroscale meteorological data in situ. The concept of temporal or solar hour is introduced. Temporal-hour at Sun rise is 00:00, at noon is 06:00 and at sunset is 12:00 in any day. Further, it is allowed to have negative values. The polynomial regression model is [11, 15]

$$C_n^2 = 5.9\times10^{-15}W + 1.6\times10^{-15}T - 3.7\times10^{-15}\mathrm{RH} + 6.7\times10^{-17}\mathrm{RH}^2 - \\ - 3.9\times10^{-19}\mathrm{RH}^3 - 3.7\times10^{-15}\mathrm{Ws} + 1.3\times10^{-15}\mathrm{Ws}^2 - 8.2\times10^{-17}\mathrm{Ws}^3 + \\ + 2.8\times10^{-14}\mathrm{SF} - 1.8\times10^{-14}\mathrm{TCSA} + 1.4\times10^{-14}\mathrm{TCSA}^2 - 3.9\times10^{-13}, \quad (5)$$

where W is temporal-hour weight values taken from [11] for computations, SF is solar flex (kWm^{-2}) and TCSA is Total Cross Section Area (cm^2/m^3). The TCSA can be determined by

$$\mathrm{TCSA} = 9.96\times10^{-4}\mathrm{RH} - 2.75\times10^{-5}\mathrm{RH}^2 + 4.86\times10^{-7}\mathrm{RH}^3 - 4.48\times10^{-9}\mathrm{RH}^4 + \\ + 1.66\times10^{-11}\mathrm{RH}^5 - 6.26\times10^{-3}\ln\mathrm{RH} - 1.37\times10^{-5}\mathrm{SF}^4 + 7.30\times10^{-3}. \quad (6)$$

This model is best one especially in practical manner since it requires only macroscale meteorological parameters which can be measured directly by a suitable weather station as in work [18]. The physical interpretation of this model can be found in papers [12, 14, 15]. The limitations of this model are Ws: 0 to 10 ms^{-1}, T: 9 to 35 °C and RH: 14 to 92% [12].

5. Model formulation and prediction accuracy confirmatory test

Obviously, the model provides a basis for making predictions about the outcomes of experiments and/or measurements. The direct methods to practical atmospheric problems are usually thwarted by the sheer size and complexity of

the atmosphere. Most of the existing models, as pointed out by several authors, are derived from the data corresponding to their local atmospheric conditions; therefore, they failed to attain the generalization on predicting the atmospheric turbulence strength [9–12]. Furthermore, these models do not offer any suitable means to tune (adapt) their parameters to fit to new test field [10, 13, 19]. Therefore, having a more accurate prediction on local turbulence strength at place of experimentation becomes significant which lead to propose the new model. The formulations of the proposed model are detailed in this section. The meteorological parameters and turbulence strength are simultaneously measured as in the paper [18] during different outdoor environmental seasons and stored in the computer. These measured values of turbulence strength (C_n^2) are related to the measured meteorological parameters using the MINITAB software and the regression analysis are performed. The data sets of size [2000×4] i.e. three input factors (Ws, T, RH) and one response factor (C_n^2) are used to formulate the regression model as explained below:

(I) Model Equation-I

$$C_n^2 = a_0 + a_1\mathrm{Ws} - a_2T - a_3\mathrm{RH} - a_4\mathrm{Ws}^2 + a_5\mathrm{Ws}T - a_6\mathrm{WsRH} + a_7T\mathrm{RH} + a_8\mathrm{Ws}^3 + a_9T^3 + a_{10}T\mathrm{RH}^2 + a_{11}\mathrm{RH}^3, \quad (7)$$

(II) Model Equation-II

$$\mathrm{C}_n^2 = b_0 - b_1\mathrm{Ws} - b_2T - b_3\,\mathrm{RH} + b_4\mathrm{Ws}^2 + b_5\mathrm{Ws}T + b_6\mathrm{WsRH} + b_7T\mathrm{RH} - b_8\mathrm{Ws}^3 + \mathrm{b}_9T^3 + b_{10}T\mathrm{RH}^2 - b_{11}\mathrm{RH}^3 + b_{12}\mathrm{Ws}^4 - b_{13}T^4 + b_{14}\mathrm{RH}^4, \quad (8)$$

(III) Model Equation-III

$$C_n^2 = c_0 - c_1\mathrm{Ws} - c_2T - c_3\mathrm{RH} + c_4\mathrm{Ws}^2 + c_5\mathrm{Ws}T + c_6\mathrm{WsRH} + c_7T\mathrm{RH} - c_8\mathrm{Ws}^3 + c_9T^3 + c_{10}T\mathrm{RH}^2 - c_{11}\mathrm{RH}^3 + c_{12}\mathrm{Ws}^4 - c_{13}\mathrm{Ws}^2T^2 - c_{14}\mathrm{Ws}^2RH^2 - c_{15}T^4 - c_{16}T^2\mathrm{RH}^2 + c_{17}\mathrm{RH}, \quad (9)$$

(IV) Model Equation-IV

$$C_n^2 = d_0 + d_1\mathrm{Ws} - d_2T - d_3\mathrm{RH} - d_4\mathrm{Ws}^2 - d_5\mathrm{Ws}T + d_6\mathrm{WsRH} - d_7T\mathrm{RH} + d_8\mathrm{Ws}^3 + d_9T^3 + d_{10}T\mathrm{RH}^2 - d_{11}\mathrm{RH}^3 + d_{12}\mathrm{Ws}^4 - d_{13}\mathrm{Ws}^3T - d_{14}\mathrm{Ws}^3\mathrm{RH} + d_{15}\mathrm{Ws}^2T^2 - d_{16}\mathrm{Ws}^2\mathrm{RH}^2 - d_{17}T^4 + d_{18}T^3\mathrm{RH} - d_{19}T^2\mathrm{RH}^2 - d_{20}\mathrm{RH}^3\mathrm{Ws} + d_{21}\mathrm{RH}^3T + d_{22}\mathrm{RH}^4, \quad (10)$$

(V) Model Equation-V

$$\mathrm{C}_n^2 = 1\times10^{-14}\big(5360.63 + 21.0442\mathrm{Ws} - 281.763\,T - 963.5576\mathrm{RH} - 0.0431099\mathrm{Ws}^2 - 0.101587\mathrm{Ws}T - 0.271695\mathrm{WsRH} + 2.19559T\mathrm{RH} - 0.26449\mathrm{Ws}^3 + 0.199294T^3 + 0.0168798T\mathrm{RH}^2 + 0.000579369\mathrm{RH}^3 - 0.001449\mathrm{Ws}^4 + 0.0101365\mathrm{Ws}^3T + 0.00092494\mathrm{Ws}^3\mathrm{RH} - 0.00159949\mathrm{Ws}^2T^2 + 0.000118693\mathrm{Ws}^2\mathrm{RH}^2 - 0.00265882\,T^4 - 0.000436822T^3\mathrm{RH} - 0.000335601T^2\mathrm{RH}^2 + 7.60425\times10^{-6}\mathrm{RH}^3\mathrm{Ws} - 6.82247\times10^{-5}\,\mathrm{RH}^3T + 1.65979\times10^{-6}\mathrm{RH}^4\big). \quad (11)$$

The individual and combined effects of the input parameters on the performance measures are analyzed and subsequently mathematical models are formulated as in Eqs. (7–11). The sensitivity of the atmospheric parameters on the turbulence strength is analyzed. The Analysis of Variable (ANOVA) tools of MINITAB are used to analyses the individual and combined effects of atmospheric parameters on the turbulence strength. Fig. 4 shows different possible combined effects of Ws, T and RH on the C_n^2.

The computed ANOVA results are used to understand the most dominating input factors on the response surface and those combinations are only considered while optimizing the model. Other regressors are insignificant and their contributions to the model's coefficient of determination (R^2) are negligible. Utmost prediction accuracy is considered while ignoring the less contributing combinations. Many models (Eqs. 7–11) were examined in order to find a model more suitable for predicting the turbulence strength as a function of meteorological parameters.

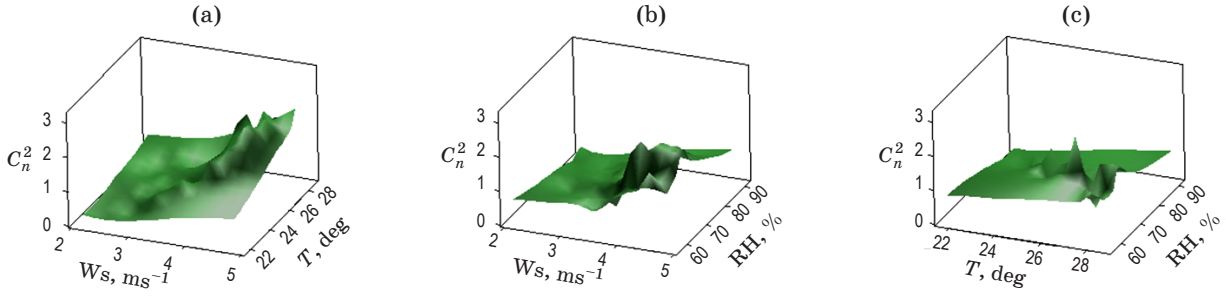

Fig. 4. Illustrations of input-output response surface plots. (a) Turbulence strength (C_n^2) vs wind speed and temperature, (b) C_n^2 vs wind speed and relative humidity and (c) C_n^2 vs temperature and relative humidity. Note that the multiplication factor in the z-axis is 10^{-14}.

The computed R^2 values of proposed turbulence strength prediction models are given against the formulated models in Table. 2. Since, the R^2 could not be computed from linear to linear + square + interaction + cubic models for C_n^2, the model equation-I to model equation-V are formulated. As in Table 2, the model equation-V, Eq. (11), exhibits the greatest correlation with the measurement values and hence, this model alone is considered for the practical implementation to predict the turbulence strength according to the local meteorological data. A portion of the residual plots obtained with the considered model, Eq. (11), for the turbulence strength is shown in Fig. 5.

Confirmatory test experiments are conducted using new set of input conditions to validate the accuracy of proposed model and a portion of outcomes of the confirmatory tests are given in Table 3. The percentage deviation (error) predicted by the proposed model are calculated by [{Experimental value − Predicted value}/Predicted value]×100.

Table 2. R^2 value of Response Surface Model (RSM) for turbulence strength prediction

Regression Model, %	R^2 value of C_n^2
Model Equation-I	78
Model Equation-II	82
Model Equation-III	89
Model Equation-IV	92
Model Equation-V	98

Table 3. Percentage deviations between experimental and prediction values of the proposed models for turbulence strength

Trial ID	Experimental $C_n^2\times10^{-12}$, m$^{-2/3}$	Predicted $C_n^2\times10^{-12}$, m$^{-2/3}$	Percentage deviation of C_n^2, %
1	0.039	0.038	2.63
2	0.417	0.418	0.23
3	0.914	0.911	0.32
4	0.249	0.243	2.46
5	0.192	0.191	0.52
6	0.078	0.075	4.00
7	0.179	0.176	1.70
8	0.731	0.733	0.27
9	0.831	0.831	0.00
10	0.294	0.291	1.03
Mean of percentage deviation			1.32

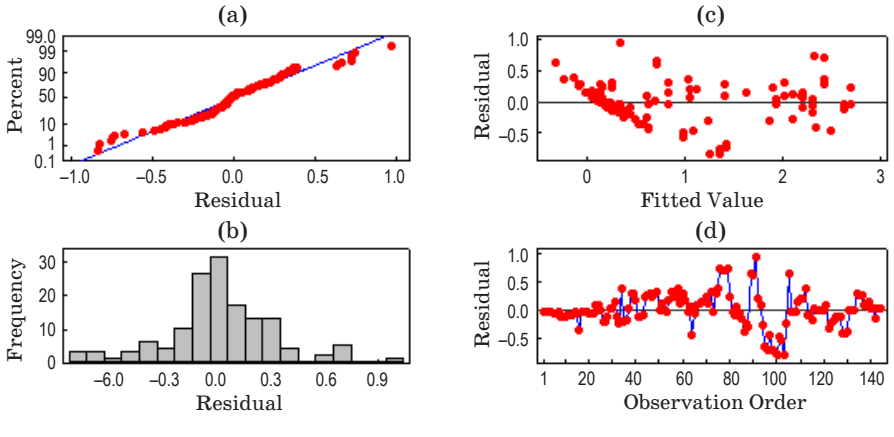

Fig. 5. Residual plots of developed regression model (Model Equation-V) for turbulence strength prediction. (a) Normal probability plot, (b) histogram, (c) versus fits, (d) versus order.

The individual and average percentage deviation results confirm the suitability of the proposed model at our test field.

6. Experimental results and data analysis

The measured meteorological data are applied as the inputs to the models discussed in section 4 and 5 and the prediction accuracy are intensively investigated. Some of the important data experimentally acquired from the real FSO link during different local seasons: pre-summer, summer, monsoon, rainy and winter at Punalkulam, Tamil Nadu in one year period are presented and from them the potential and feasibility of all the selected and proposed models are evaluated. The diurnal period performance of meteorological parameter is studied in terms of minimum and maximum (min-max) values and standard deviation (Std). The outstanding performance of the proposed model in predicting the turbulence strength is assessed and the results are presented in this section. The local meteorological data and turbulence strength are measured as in paper [18] for every second in the diurnal periods and averaged data are recorded and the environmental changes are studied. The necessary data and measured values of meteorological, beam centroid information, temporal-hour weight, geographical, geometrical and received beam parameters are substituted in Eqs. (1–6, 11) as required and prediction results are compared against the measured C_n^2 [18]. The selected and proposed models are implemented in MATLAB environment. The accuracies of the prediction of the models are carefully analyzed in terms of SAE. The profile of recorded real time meteorological data and prediction & measurement values of turbulence strength are described below for five days chosen somewhat randomly in different local seasons, since FSOC is mainly season dependent, in one year period.

6.1 Data for 16th March 2013 – Pre-summer

The weather parameters variations from 0.27 to 6.18 ms^{-1} with the Std of 1.50 ms^{-1} for Ws, 25 to 36.11 °C with the Std of 3.60 °C for T, 30 to 83% with the Std of 14.64% for RH and 101.1 to 101.6 kPa with the Std of 0.14 kPa for P are observed from Figs. 6 (a–d). The Std on the T and RH are high; Ws and P are relatively low. The different conditions of the atmosphere observed on 16th March 2013 (Saturday) are partially cloudy, hazy, scattered cloudy and mostly cloudy. Uneven Ws and RH variations are observed as in Fig. 6a and 6c respectively.

Fig. 7a shows the experimental time series plot of C_n^2 predicted from local meteorological data collected on 16th March 2013 and measured values. The min-max values of measured C_n^2 are near 2.36×10^{-14} and 2.01×10^{-13} $m^{-2/3}$ about early morning and noon (Nn) respectively with the Std of 5.90×10^{-14} $m^{-2/3}$ when Ws, T are low: 0.27ms^{-1}, 25 °C and RH is high: 83%.

The min-max values of C_n^2 predicted by the PAMELA model are 5.46×10^{-20} and 2.23×10^{-10} $m^{-2/3}$ about 5.30 p.m and 6.45 a.m when Ws, T are high: 5.1 ms^{-1}, 35 °C; RH, P are low: 38%, 101.1 kPa and Ws, T, P are low: 0.2 ms^{-1}, 25 °C, 101.2 kPa; RH is high: 80% respectively. Local minima are seen in the early morning and late evening at 7.14×10^{-16} and 5.46×10^{-20} $m^{-2/3}$ about 4.20 a.m, 5.30 p.m respectively. A greatly fluctuating turbulence pattern is predicted by PAMELA model during 6.00 a.m to 6.45 p.m, since the model keeps high sensitivity to Ws. The results yield less correlation with the measurements

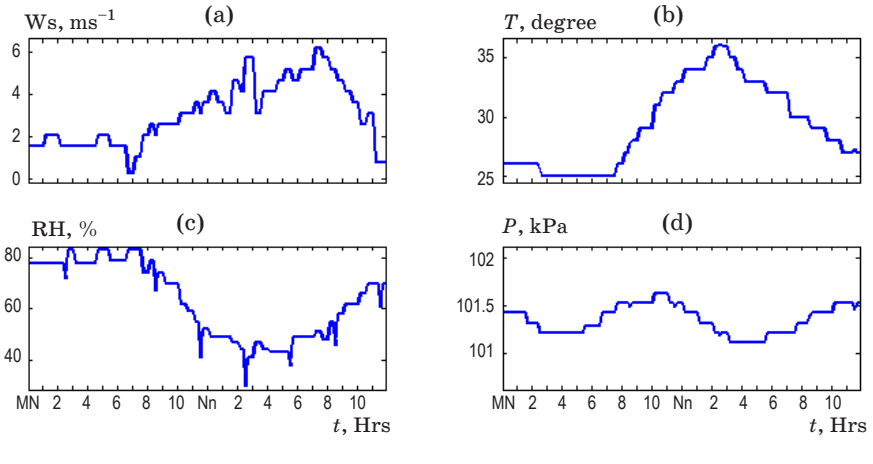

Fig. 6. Diurnal time series updation of meteorological parameters-wind speed (a), temperature (b), relative humidity (c) and barometric pressure (d). t – local time (GMT + 5.30) of the day.

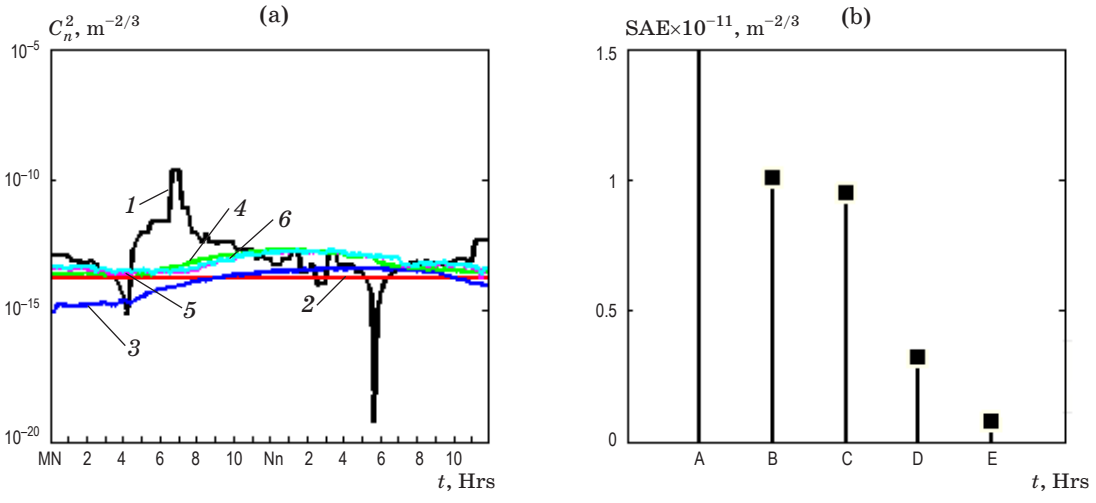

Fig. 7. Graphical comparison of time series updation of atmospheric turbulence strength (C_n^2) predicted using selected and proposed models and measured from direct beam transmission system (a). Models: *1* – PAMELA, *2* – Hufnagel-Valley, *3* – beam wandering, *4* – polynomial regression, *5* – proposed; *6* – measurement. Sum of absolute error value against the particular model (b). Models: A – PAMELA ($x = 1$, $y = 0.7310 \times 10^{-9}$), B – Hufnagel-Valley ($x = 2$, $y = 1.0085 \times 10^{-11}$), C – beam wandering ($x = 3$, $y = 9.5077 \times 10^{-12}$), D – polynomial regression ($x = 4$, $y = 3.1984 \times 10^{-12}$), E – proposed ($x = 5$, $y = 7.4059 \times 10^{-13}$). t – local time (GMT + 5.30) of the day.

almost all the time of the day except few instances at 3.32×10^{-14}, 2.74×10^{-14}, 1.80×10^{-13}, 1.99×10^{-13} and 4.751×10^{-14} m$^{-2/3}$ about around 3.00 a.m, 4.15 a.m, 11.15 a.m, 3.10 p.m and 8.00 p.m respectively as shown in Fig. 7a. The maximum deviation is 2.22×10^{-10} m$^{-2/3}$ and therefore, this model cannot be used to get accurate prediction of the C_n^2 at our test field. The min-max value of C_n^2 predicted by the Hufnagel-Valley model is 1.65×10^{-14} m$^{-2/3}$ with the Std of 1.9×10^{-29} m$^{-2/3}$ i.e this model yields a constant C_n^2 (singularity) throughout the day as in Fig. 7a with the maximum deviation of 1.67×10^{-13} m$^{-2/3}$. This result clearly exhibits that this model could not keep much dependency to the Ws variations at the 15.25 m altitude and may yield reasonable results as a function of higher altitude. This model shows somewhat good correlation at 3.02×10^{-14} m$^{-2/3}$ about 4.00 a.m in this season. However this model is unfit at our test field.

The min-max values of C_n^2 predicted based on beam wandering are 8.6×10^{-16} and 4.29×10^{-14} m$^{-2/3}$ respectively with the Std of 1.44×10^{-14} m$^{-2/3}$ about mid night (MN) and 2.30 p.m to 6.00 p.m when the Ws, T are low: 1.5 ms^{-1}, 26 °C; RH, P are high: 78%, 101.4 kPa and Ws, T are high: 5.9 ms^{-1}, 35 °C; RH, P are low: 44%, 101.1 kPa respectively. The model predicts a smooth turbulence pattern roughly similar to measurement with a maximum deviation of 4.87×10^{-14} m$^{-2/3}$ as in Fig. 7a. The results meet the measurements at 5.20×10^{-14} m$^{-2/3}$ about 6.50 p.m, when Ws, T, P are normal: 4.5 ms^{-1}, 32 °C, 101.2 kPa and RH is low: 50%. This model is unsuitable at our test field. The min-max values of polynomial regression model are 2.03×10^{-14} m$^{-2/3}$ and 2.03×10^{-13} m$^{-2/3}$ respectively with the Std of 6.32×10^{-14} m$^{-2/3}$ about MN and 11.00 a.m to 4.00 p.m when Ws, T are low: 1.5 ms^{-1}, 26 °C; RH is high: 78% and Ws, T keep increasing while RH decreases as in Figs. 6(a–c). This model exhibits a good correlation throughout the day in this season as in Fig. 7a except few instances at 4.19×10^{-14}, 7.26×10^{-14}, 1.05×10^{-13} and 3.99×10^{-14} m$^{-2/3}$ about 1.30 a.m, 7.45 a.m, 6.15 p.m and 11.05 p.m respectively with the maximum deviation of 5.47×10^{-14} m$^{-2/3}$. The min-max values of the proposed model are 2.35×10^{-14} and 1.94×10^{-13} m$^{-2/3}$ respectively with the std of 5.91×10^{-14} m$^{-2/3}$ about MN and 11.15 a.m to 3.50 p.m when the Ws, T are low: 1.5 ms^{-1}, 26 °C; RH is high: 78% and Ws, T keep increasing while RH decreases as in Figs. 6(a–c) and Fig. 7a. The proposed model yields a great correlation with the measurements all the time of the day. The computed SAE using the measured and predicted values are shown in Fig. 7b against the respective model and prove that the proposed model gives very less SAE of 7.40×10^{-13} m$^{-2/3}$ whereas the other models are 0.7310×10^{-9}, 1×10^{-11}, 9.50×10^{-12} and 3.19×10^{-12} m$^{-2/3}$.

6.2 Data for 31st May 2013 – Summer

The weather parameters variations from 0.27 to 6.16 ms^{-1} with the Std of 1.42 ms^{-1} for Ws, 26 to 36 °C with the Std of 3 °C for T, 39 to 89% with the Std of 14.54% for RH and 100.3 to 100.7 kPa with the Std of 0.128 kPa for P are observed from Figs. 8(a–d).

The Std of RH is significantly high while Ws, T and P are low. The different conditions of the atmosphere observed on 31st May 2013 (Friday) are mostly cloudy, hazy, scattered cloudy, partial cloudy and light drizzle. The Ws oscillates randomly around 2.59 ms^{-1} in forenoon and 4.11ms^{-1} in afternoon. Fig. 9a shows the experimental time series plot of C_n^2 predicted from local meteorological data collected on 31st May 2013 and measured values. The min-max values of measured C_n^2 are near 1.35×10^{-14} and 1.94×10^{-13} $m^{-2/3}$ about MN and 10.00 a.m to 4.30 p.m respectively with the Std of 5.61×10^{-14} $m^{-2/3}$ when Ws, T are low: 1.02 ms^{-1}, 27 °C; RH is high: 89% and Ws is normal: 3.08 ms^{-1}; T is high: 37 °C; RH is low: 60% as in Figs. 8(a–c). Sustained and smooth steady variations are seen in the measured turbulence pattern. In comparison of selected models: The min-max values of C_n^2 predicted by the PAMELA model are 2.138×10^{-17} and 2.178×10^{-10} $m^{-2/3}$ with the Std of 4.27×10^{-11} $m^{-2/3}$ about 5.05 p.m and 7.10 a.m & 1.13 p.m respectively. Local minima existed in the early morning and late evening at 3.90×10^{-17} and 2.13×10^{-17} $m^{-2/3}$ about 4.05 a.m and 5.05 p.m respectively. A greatly sporadic C_n^2 pattern is predicted with the maximum deviation of 1.21×10^{-13} $m^{-2/3}$ since unrealistically fluctuations are seen in the meteorological variations (except pressure). The prediction results hold poor correlation with the measurements in gener-

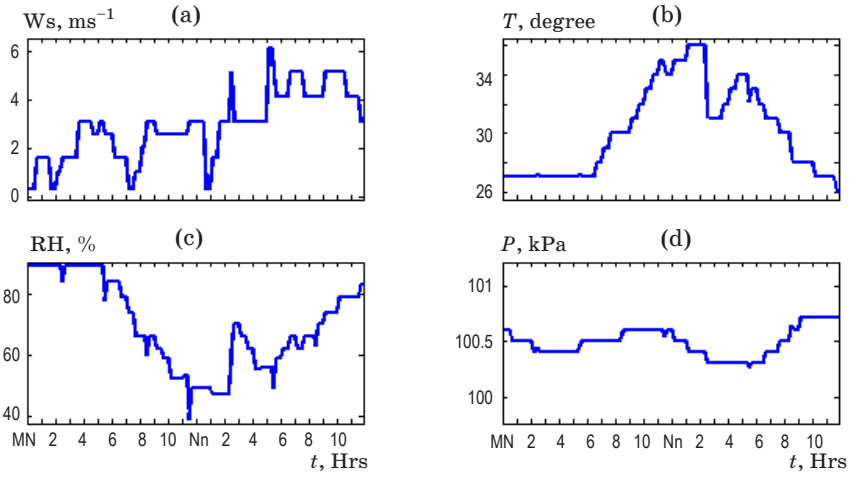

Fig. 8. Same as Fig. 6 except on 31st May 2013.

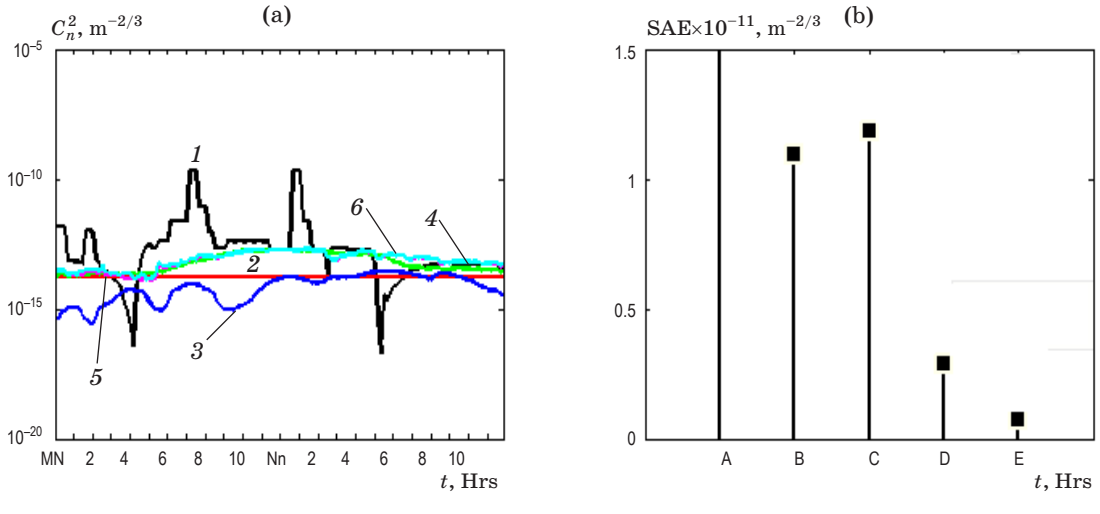

Fig. 9. Same as Fig. 7 except on 31st May 2013. A – $x = 1$, $y = 0.13 \times 10^{-8}$, B – $x = 2$, $y = 1.0937 \times 10^{-11}$, C – $x = 3$, $y = 1.1847 \times 10^{-11}$, D – $x = 4$, $y = 3.0763 \times 10^{-12}$, E – $x = 5$, $y = 6.989 \times 10^{-13}$.

al and meet it randomly at 2.77×10^{-14}, 2.37×10^{-14}, 1.92×10^{-13}, 9.75×10^{-14} and 1.55×10^{-13} $m^{-2/3}$ about 2.45 a.m, 4.30 a.m, 1.00 p.m, 1.55 p.m and 5.00 p.m respectively as in Figs. 8(a–d) and Fig. 9a. A close correlation is seen from 8.45 p.m onwards when the Ws is normal: 4 ms^{-1}; T is low: 28 °C, RH is high: 79% and P is high: 100.7 kPa.

The min-max values of Hufnagel-Valley model is 1.65×10^{14} $m^{-2/3}$ with the Std of 1.9×10^{-29} $m^{-2/3}$ i.e. a constant C_n^2 is predicted throughout the day. This model exhibits a reasonable fit with the measurements at 2.59×10^{-14} $m^{-2/3}$ from MN to 5.05 a.m. The deflection began 5.05 a.m onwards with the maximum value of 1.50×10^{-13} $m^{-2/3}$. The min-max values of beam wandering model are 2.60×10^{-16} and 2.84×10^{-14} $m^{-2/3}$ with the Std of 8.50×10^{-15} $m^{-2/3}$ about MN and 5.15 p.m respectively. The prediction results always fall below the measurements with the maximum deviation of 1.46×10^{-13} $m^{-2/3}$. An oscillating pattern of C_n^2 is seen in forenoon due to the greatest fluctuations in the Ws as in Fig. 9a and Fig. 8a. The deviation decreases in the afternoon and becomes close to results predicted by the Hufnagel-Valley model. The min-max values of polynomial regression model are 1.74×10^{-14} and 1.93×10^{-13} $m^{-2/3}$ with the Std of 6×10^{-14} $m^{-2/3}$ respectively around MN and 10.00 a.m to 2.00 p.m when Ws fluctuates about 2.59 ms^{-1}, T increases: 30 to 36 °C and RH decreases: 62 to 47% as in Figs. 8(a–c). This model keeps a good track on measurements from MN to 5.15 p.m and the deviation began with the maximum deviation of 3.5×10^{-14} $m^{-2/3}$. The min-max values of proposed model are 1.37×10^{-14} and 1.87×10^{-13} $m^{-2/3}$ with the Std of 5.64×10^{-14} $m^{-2/3}$ about MN and 10.00 a.m to 2.10 p.m respectively. The proposed model exhibits a greater correlation with the measurements as shown in Fig. 9a. The SAE results shown in Fig. 9b proves that the proposed model exhibits a very less value of 6.98×10^{-13} $m^{-2/3}$ whereas other models are 0.134×10^{-8}, 1.0910^{-11}, 1.18×10^{-11} and 3.07×10^{-12} $m^{-2/3}$.

6.3. Data for 14th June 2013 – Monsoon

The weather parameters variations from 4.11 to 10.82 ms^{-1} with the Std of 2.09 ms^{-1} for Ws, 28 to 36 °C with the Std of 2.73 °C for T, 25 to 62% with the Std of 9.62% for RH and 100 to 100.4 kPa with the Std of 0.11 kPa for P are observed from Figs. 10(a–d). The Std on the RH is significantly large while the Ws, T and P are very low. The different conditions in the atmosphere observed on 14th June 2013 (Friday) are light drizzle, drizzle and hazy. Greatly uneven Ws variation is observed as in Fig. 10a.

Fig.11a shows the experimental time series plot of C_n^2 predicted from local meteorological data collected on 14th June 2013 and measured values. The min-max values of measured C_n^2 are near 3.63×10^{-14} and 1.87×10^{-13} $m^{-2/3}$ about MN and 11.00 a.m to 12.30 p.m respectively with the Std of 4.50×10^{-14} $m^{-2/3}$ when the Ws, T, P are low: 5.1 ms^{-1}, 29 °C, 100.1 kPa; RH is high: 62% and Ws, T, P are high: 10.82 ms^{-1}, 35 °C, 100.34 kPa; RH is low: 39%. In comparison of selected models: The min-max values of C_n^2 predicted by the PAMELA model are 4.47×10^{-18} and 3.21×10^{-13} $m^{-2/3}$ with the Std of 8.78×10^{-14} $m^{-2/3}$ respectively about 4.30 a.m and 11.50 p.m. Local minima are obtained at 4.47×10^{-18} and 8.39×10^{-18} $m^{-2/3}$ about 4.20 a.m and 4.00 p.m respectively. The prediction results fall below the measurements almost all the time and fall above from 6.00 p.m to MN with the maximum deviation of 1.49×10^{-13} $m^{-2/3}$.

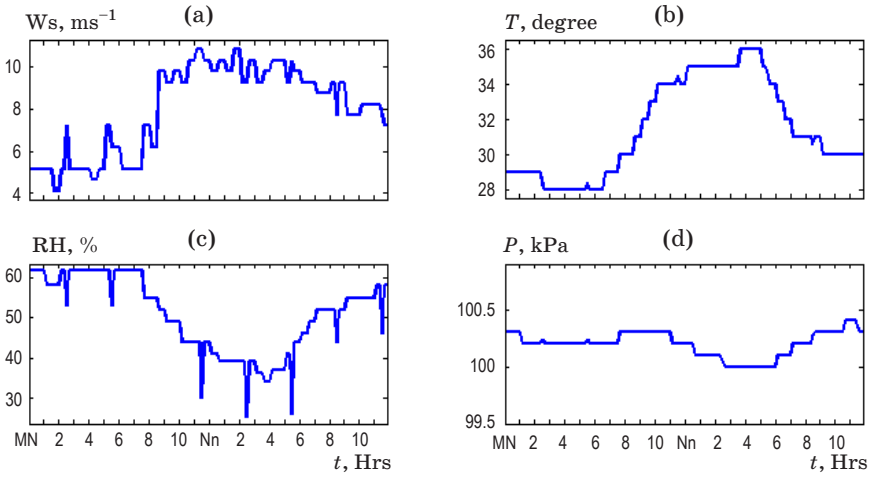

Fig. 10. Same as Fig. 6 except on 14th June 2013.

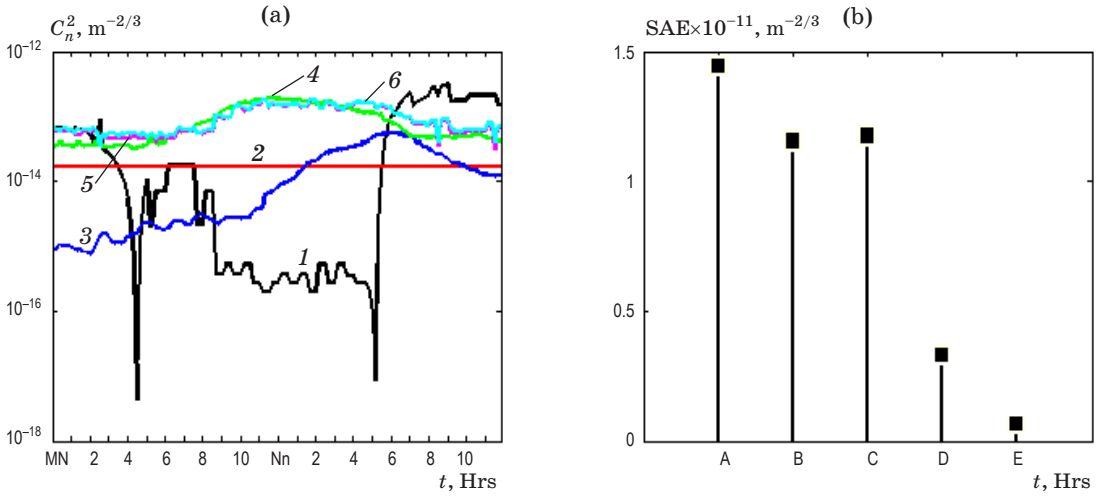

Fig. 11. Same as Fig. 7 except on 14th June 2013. A – $x = 1$, $y = 1.4378 \times 10^{-11}$, B – $x = 2$, $y = 1.1546 \times 10^{-11}$, C – $x = 3$, $y = 1.1724 \times 10^{-11}$, D – $x = 4$, $y = 3.3178 \times 10^{-12}$, E – $x = 5$, $y = 6.9344 \times 10^{-13}$.

The results keep reasonable correlation around 1.30 a.m since Ws, T are low: 5.1 ms^{-1}, 29 °C and RH, P are high: 62%, 100.3 kPa. The great fluctuations in Ws yield the unrealistically large sporadic C_n^2 pattern in day time as in Figs. 10a and 11a.

The min-max values of the C_n^2 predicted by the Hufnagel-Valley are 1.658×10^{-14} m$^{-2/3}$ with the Std of 1.9×10^{-29} m$^{-2/3}$ i.e a constant C_n^2 is given by the model throughout the day. The prediction results are immaterial with measurements with the maximum deviation of 1.65×10^{-14} m$^{-2/3}$ as in Fig. 11a. The min-max values of the C_n^2 predicted by the beam wandering model are 7.36×10^{-16} and 5.4×10^{-14} m$^{-2/3}$ with the Std of 1.66×10^{-14} m$^{-2/3}$ about MN and 4.15 p.m to 7.00 p.m. The results very slowly increase to the maxima from MN to 6.40 p.m and decrease to minima. The results fall below the measurements throughout the day with the maximum deviation of 6.52×10^{-14} m$^{-2/3}$. The correlation between prediction and measurement are immaterial as in Fig. 11a.

The min-max values of C_n^2 predicted by polynomial regression model are 3.31×10^{-14} and 2×10^{-13} m$^{-2/3}$ with the Std of 5.51×10^{-14} m$^{-2/3}$ about MN and 11.00 a.m to 4.00 p.m respectively when the Ws, T are low: 5.14 ms^{-1}, 29 °C; RH is high: 62% and Ws, T are high: 10.82 ms^{-1}, 36 °C; RH is low: 38%. The prediction results fail to maintain good correlation with the measurements throughout the day unlike its behavior in the previous seasons. The results appear above the measurements from 7.00 a.m to 2.00 p.m with the maximum deviation of 8.7×10^{-14} m$^{-2/3}$. However the results fall below with the greater deviations during MN to 6.00 a.m and 3.00 p.m to MN as in Fig. 11a. The min-max values of proposed model are 3.18×10^{-14} and 1.7×10^{-13} m$^{-2/3}$ with the Std of 4.46×10^{-14} m$^{-2/3}$ about MN and 11.00 a.m to 3.30 p.m respectively. The proposed model exhibits a greater correlation with the measurements as in shown Fig. 11a. The SAE results shown in Fig. 11b proves that the proposed model exhibits a very less value of 7.27×10^{-13} m$^{-2/3}$ whereas other models are 0.14×10^{-10}, 8.77×10^{-12}, 1.01×10^{-11} and 5.28×10^{-12} m$^{2/3}$.

6.4. Data for 21st November 2013 – Rainy

The weather parameters variations from 0.25 to 4.11 ms^{-1} with the Std of 0.90 ms^{-1} for Ws, 25.2 to 31.36 °C with the Std of 2.26 °C for T, 55 to 94% with the Std of 11.67% for RH and 100.5 to 101 kPa with the Std of 0.146 kPa for P are observed from Figs. 12(a–d). The Std of the T and RH are high while Ws and P are low. The different conditions of the atmosphere observed on 21st November 2013 (Thursday) are hazy, scattered cloudy, fogy and misty.

Fig. 13a shows the experimental time series plot of C_n^2 predicted from local meteorological data collected on 21st November 2013 and measured values. The min-max values of measured C_n^2 are approximately 3.43×10^{-14} and 1.40×10^{-13} m$^{-2/3}$ about MN and 11.00 a.m to 4.00 p.m respectively with the Std of 3.20×10^{-14} m$^{-2/3}$. In comparison of selected models: The min-max values of C_n^2 predicted by PAMELA model are 4.82×10^{-17} and

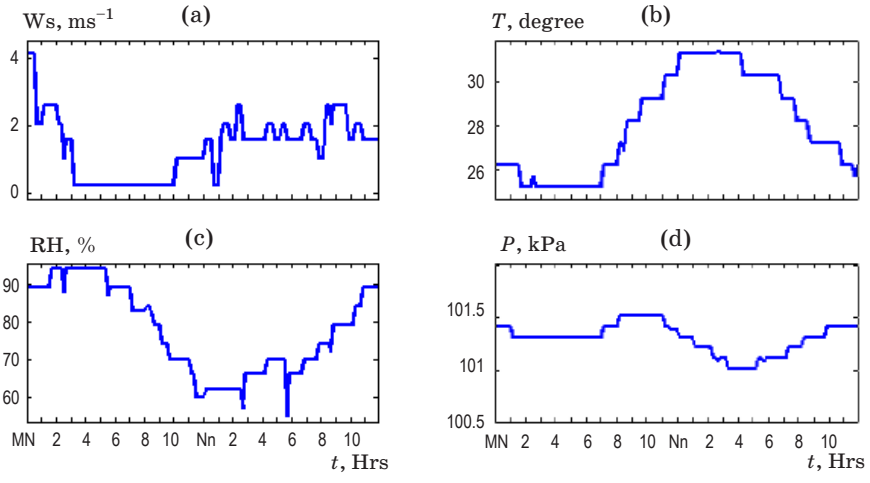

Fig. 12. Same as Fig. 6 except on 21st November 2013.

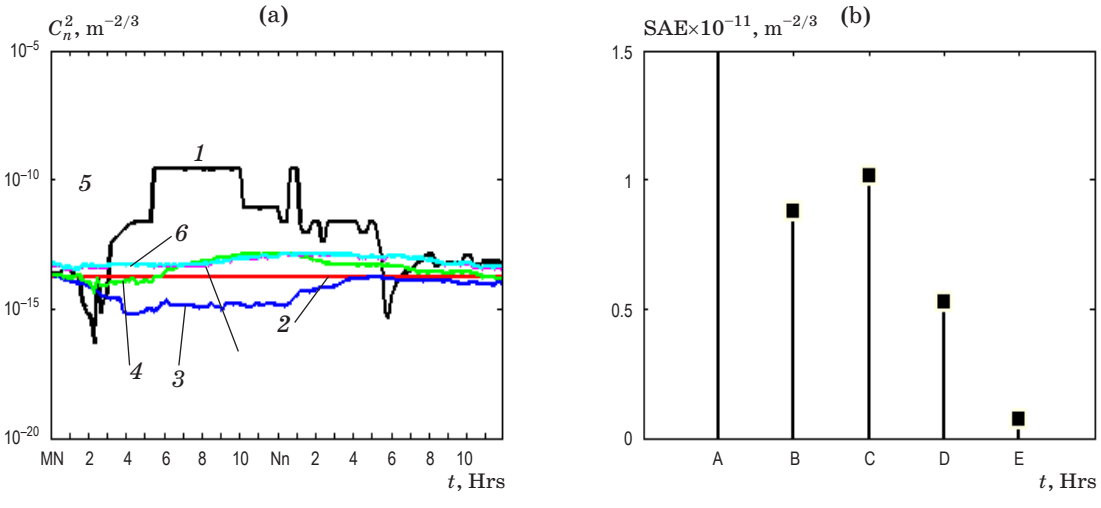

Fig. 13. Same as Fig. 7 except on 21st November 2013. A – $x = 1$, $y = 0.81 \times 10^{-8}$, B – $x = 2$, $y = 8.7721 \times 10^{-12}$, C – $x = 3$, $y = 1.0164 \times 10^{-11}$, D – $x = 4$, $y = 5.2832 \times 10^{-12}$, E – $x = 5$, $y = 7.2768 \times 10^{-13}$.

2.60×10^{-10} m$^{-2/3}$ with the Std of 1.05×10^{-10} m$^{-2/3}$ about 2.10 a.m and 5.10 a.m to 10.05 a.m respectively. The prediction results are highly sporadic as like the Ws in Fig. 12a.

Most of the time, the results fall above the measurements as in Fig. 13a with the maximum deviation of 2.56×10^{-10} m$^{-2/3}$. This model exhibits local minima at 4.82×10^{-17} and 4.68×10^{-16} m$^{-2/3}$ about 2.05 a.m and 5.55 p.m respectively with the reasonable correlation during 8.00 p.m to MN since Ws is calm: 0.27 ms^{-1}, T is low: 26.21 °C, RH is high: 90% and P is high: 100.9 kPa. The min-max value of the C_n^2 predicted by the Hufnagel-Valley is 1.658×10^{-14} m$^{-2/3}$ with the Std of 1.9×10^{-29} m$^{-2/3}$ i.e. a constant C_n^2 is given by the model throughout the day and appears above the measurements. The prediction results are immaterial with measurements with the maximum deviation of 1.23×10^{-13} m$^{-2/3}$ as in Fig. 13a. The min-max values of C_n^2 predicted by beam wandering model are 6.13×10^{-16} and 1.94×10^{-14} m$^{-2/3}$ with Std of 5.60×10^{-15} m$^{-2/3}$ about 4.10 a.m and 5.05 p.m respectively. The prediction results appear below the measurements with the maximum deviation of 5.32×10^{-14} m$^{-2/3}$. The deviation decreases from 1.00 p.m onwards and become close to the response of Hufnagel-Valley model. However, the prediction results are irrelevant to the measurements throughout the diurnal period. The min-max values of C_n^2 predicted by polynomial regression model are 3.98×10^{-15} and 1.42×10^{-13} m$^{-2/3}$ with the Std of 4.04×10^{-14} m$^{-2/3}$ about MN and 10.00 a.m to 4.00 p.m respectively. This model exhibits a reasonable correlation with the measurements in forenoon session from 7.00 a.m to 1.00 p.m and apart, the deviation exists with the maximum value of 4.62×10^{-14} m$^{-2/3}$ as its behavior in the

previous season. The min-max values of proposed model are 3.35×10^{-14} and 1.31×10^{-13} $m^{-2/3}$ with the Std of 3.22×10^{-14} $m^{-2/3}$ about MN and 10.30 a.m to 4.30 p.m respectively. The proposed model exhibits a greater correlation with the measurements as shown in Fig. 13a. The SAE results shown in Fig. 13b indicate that the proposed model exhibits a very less value is 6.93×10^{-13} $m^{-2/3}$ whereas other models are 0.81×10^{-8}, 1.15×10^{-11}, 1.17×10^{-11} and 3.31×10^{-12} $m^{-2/3}$.

6.5. Data for 25th December 2013 – Winter

The weather parameter variations from 2.05 to 7.19 ms^{-1} with the Std of 1.30 ms^{-1} for Ws, 22.18 to 30.24 °C with the Std of 2.59 °C for T, 40 to 88% with the Std of 11.28% for RH and 101.3 to 101.8 kPa with the Std of 0.11 kPa for P are observed from Figs. 14(a–d). The Std of the T and RH are high while Ws and P are low. The different conditions of the atmosphere observed on 25th December 2013 (Wednesday) are hazy, partially cloudy, misty and scattered cloudy.

Fig. 15a shows the experimental time series plot of C_n^2 predicted from local meteorological data collected on 25th December 2013 and measured values. The min-max values of measured C_n^2 are approximately 1.13×10^{-14} and 8.34×10^{-14} $m^{-2/3}$ respectively about MN and 9.00 a.m to 4.00 p.m with the Std of 2.06×10^{-14} $m^{-2/3}$ when Ws, T are low: 2.5 ms^{-1}, 24.19 °C; RH, P are high: 78%, 101.6 kPa and Ws, T are high: 6.19ms^{-1}, 30.24 °C; RH, P are low: 50%, 101.2 kPa. The larger fluctuations in the meteorological values generate unrealistically large sporadic C_n^2 values. In comparison of selected models: The min-max values of C_n^2 predicted by PAMELA model are 3.68×10^{-17} and 4.17×10^{-13} $m^{-2/3}$ with the Std

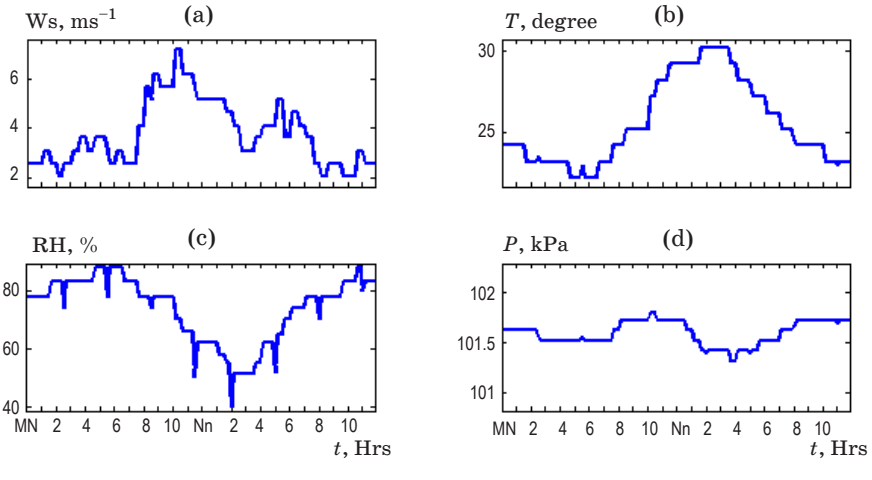

Fig. 14. Same as Fig. 6 except on 25th December 2013.

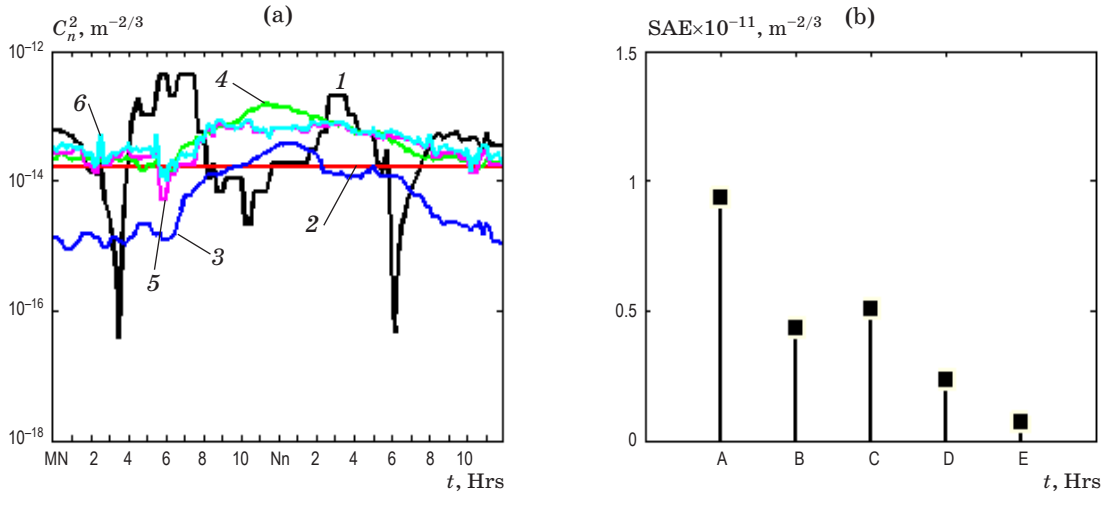

Fig. 15. Same as Fig. 7 except on 25th December 2013. A – $x = 1$, $y = 9.3534 \times 10^{-12}$, B – $x = 2$, $y = 4.1733 \times 10^{-12}$, C – $x = 3$, $y = 5.0954 \times 10^{-12}$, D – $x = 4$, $y = 2.4641 \times 10^{-12}$, E – $x = 5$, $y = 7.3512 \times 10^{-13}$.

of 1.03×10^{-13} $m^{-2/3}$ about 3.15 a.m and around 7.00 a.m respectively. The prediction results did not match with the measurements and the maximum deviation is 4.00×10^{-13} $m^{-2/3}$. Two local minima exist at 3.68×10^{-17} and 4.74×10^{-17} $m^{-2/3}$ about 3.15 a.m and 6.00 p.m respectively as in Fig. 15a. The prediction pattern approximately, oscillates about the measurements. The C_n^2 pattern clearly exhibits the greatest dependency of the PAMELA model to the Ws. The min-max values of the C_n^2 predicted by the Hufnagel-Valley is 1.65×10^{-14} $m^{-2/3}$ with the Std of 1.9×10^{-29} $m^{-2/3}$ i.e. a flat behavior with a constant C_n^2 is given by the model throughout the day and appears below the measurements. The prediction results are immaterial with measurements with the maximum deviation of 5.35×10^{-14} $m^{-2/3}$ as in Fig. 15a.

The min-max values of C_n^2 predicted by beam wandering model are 8.69×10^{-16} and 3.78×10^{-14} $m^{-2/3}$ with the Std of 1.03×10^{-14} $m^{-2/3}$ about MN and Nn respectively. A sustained and steady increased and decreased C_n^2 pattern is seen throughout the diurnal period as in Fig. 15a. The result exhibits approximately the same pattern as the measurements with a maximum deviation of 3.14×10^{-14} $m^{-2/3}$. However, the results fall below the measurements throughout the day. The min-max values of C_n^2 predicted by the polynomial regression model are 1.38×10^{-15} and 1.49×10^{-13} $m^{-2/3}$ about MN and 11.00 a.m to 1.30 p.m respectively. The prediction results yield a reasonable correlation with the measurements from MN to 9.00 a.m and 3.00 p.m to MN. A greatest deviation existed around Nn with the maximum deviation of 8.43×10^{-14} $m^{-2/3}$. The results absolutely match the measurements only for some instance at 2.19×10^{-14}, 1.29×10^{-14}, 7.49×10^{-14}, 5.83×10^{-14} and 4.86×10^{-14} $m^{-2/3}$ about 2.00 a.m, 6.05 a.m, 9.05 a.m, 3.45 p.m and 6.05 p.m respectively as in Fig. 15a. The min-max values of proposed model are 5.11×10^{-15} and 7.58×10^{-13} $m^{-2/3}$ with the Std of 2.05×10^{-14} $m^{-2/3}$ about MN and 10.00 a.m to 3.45 p.m respectively. The proposed model exhibits a greater correlation with the measurements as shown in Fig. 15a. The SAE results shown in Fig. 15b evidence that the proposed model exhibits a very less value of 7.35×10^{-13} $m^{-2/3}$ whereas other models are 0.93×10^{-11}, 4.17×10^{-12}, 5.09×10^{-12} and 2.46×10^{-12} $m^{-2/3}$.

7. Conclusions

The significance of model design for C_n^2 prediction is explained along with the measurement technique and estimation of received beam centroid information. The literature review results of background and related works are presented. The establishment of experimental setups (transmitter and receiver) built for model development and practical validation are explained. The models selected for comparative analysis are briefed. The formulation of empirical model are detailed and based on the results of coefficient of determination (R^2) obtained from ANOVA tools, the Eq. (11), R^2 = 98%, is finalized for turbulence strength prediction. Average percentage deviation of 1.32% is obtained for turbulence strength from the confirmatory test. The seasonal average SAE of 7.40×10^{-13}, 6.98×10^{-13}, 7.27×10^{-13}, 6.93×10^{-13}, 7.35×10^{-13} $m^{-2/3}$ are achieved during five different seasons: pre-summer, summer, monsoon, rainy and winter respectively in one year period. These results evidence the suitability and feasibility of the proposed model to have more accurate prediction results at our test field throughout the duration of experimentations.

* * * * *

ЛИТЕРАТУРА

1. *Brandenburg J.C.* Signal detection for optical communications through the turbulent atmosphere // IEEE Trans. Commun. 2009. V. 57. № 11. P. 3425–3432.
2. *GappmairA.A.* Further results on the capacity of free-space optical channels in turbulent atmosphere // IET Commun. 2011. V. 5. Iss. 9. P. 1262–1267.
3. *Raj A.B., Selvi A.A.V., Kumar J. D., and Raghavan S.* Intensity feedback-based beam wandering mitigation in free-space optical communication using neural control technique // EURASIP Journal on Wireless Communications and Networking. 2014. V. 160. P. 1–18.
4. *Ni W., Miyamoto Y., Wakamori K., Kazaura K., Matsumoto M., Higashino T., Tsukamoto K., and Komaki S.* Experimental study of atmospheric turbulence effects on RoFSO communication systems // PIERS Online. 2009. V. 5. № 1. P. 65–70.

5. *Silva V.N.H., Barbero A.P.L., and Ribeiro R.M.* A new triangulation-like technique for the evaluation of the refractive index structure constant (C_n^2) in free-space optical links // J. Lightwave Technol. 2011. V. 29. № 24. P. 3603–3610.

6. *Zamek S. and Yitzhaky Y.* Turbulence strength estimation from an arbitrary set of atmospherically degraded images // J. Opt. Soc. America A. 2006. V. 23. № 12. P. 3106–3113.

7. *Tunick A.* Optical turbulence parameters characterized via optical measurements over a 2.33 km free-space laser path // Opt. Exp. 2008. V. 16. Iss.19. P. 14645–14654.

8. *Mudge K.A., Silva K.K.M.B.D., Clare B.A., Grant K.J., and Nener B.D.* Scintillation Index of the free space optical phase screen modeling and experimental results // International. Conf. "Space Optical Systems and Applications". Santa Monica, 2011. P. 403–409.

9. *Recolons J., Andrews L.C., and Philips R.L.* Analysis of beam wander effects for a horizontal-path propagating gaussian-bam wave: Focused beam case // Opt. Eng. 2007. V. 46. № 8. P. 1–11.

10. *Raj A.A.B., Selvi J.A.V.* Comparison of different models for ground-level atmospheric attenuation prediction with new models according to local weather data for FSO applications // J. Opt. Commun. 2015. V. 54. Iss. 4. P. 802–815.

11. *Leclerc T.T., Philips R.L., Andrews L.C., Wayne D.T., Saucer P., and Crabbs R.* Prediction of the ground-level refractive index structure parameter from the measurement of atmospheric conditions // SPIE Conf. "Atmospheric Propagation VII". Florida, 2010. Part. 7685. P. 1–8.

12. *Sadot D., Kopeika N.S.* Forecasting optical turbulence strength on the basis of macroscale meterology and aerosols: Models and validation // Opt. Eng. 1992. V. 31. № 2. P. 200–212.

13. *Doss-Hammel S., Oh E., Ricklin J., Eaton F., Gilbert C., Tsintikidis D.* A comparison of optical turbulence model // SPIE Conf. "Free-Space Laser Communications IV". Denver, CO, 2004. Part 5550. P. 236–245.

14. *Yitzhaky Y., Dror I., and Kopeika N.S.* Restoration of atmospherically blurred images according to weather-predicted atmospheric modulation transfer functions // Opt. Eng. 1997. V. 36. № 11. P. 3064–3072.

15. *Bendersky S., Kopeika N.S., and Blaunstein N.* Atmospheric optical turbulence over land in Middle East coastal environments: Prediction modeling and measurements // Appl. Opt. 2004. V. 43. № 20. P. 4070–4079.

16. *Monin A.S. and Obukhov A.M.* Basic law of turbulent mixing near the ground // J. Geophysical Institute of Slovak Academy of Sciences, USSAR. 1954. V. 24. № 151. P. 163–187.

17. *Majumdar A.K., Eaton F.D., Jensen M.L., Kyrazis D.T., Schumm B., Dierking M.P., Shoemake M.A., Dexheimer D., and Ricklin J.C.* Atmospheric turbulence measurements over desert site using ground-based instruments, kite/tethered – blimp platform and aircraft relevant to optical communications and imaging systems: Preliminary results // SPIE Conf. "Free-Space Laser Communications VI". San Diego, California, USA, 2006. Part 6304. P. 1–12.

18. *Raj A.A.B., Selvi J.A.V., and Raghavan S.* Real-time measurement of meteorological parameters for estimating low-altitude atmospheric turbulence strength (C_n^2) // IET Science, Measurement & Technology. 2014. V. 8. Iss. 6. P. 459–469.

19. *Randall D.* An introduction to atmospheric modeling. USA, Colorado State University, 2004.

20. *Arockia Bazil A., Selvi J.A.V., Kumar D., Raghavan S.* Design of cognitive decision making controller for autonomous online adaptive beam steering in free space optical communication system // Wireless Personal Communications. 2015. V. 84. № 1. P. 765–799.

21. *Tunick A.* Statistical analysis of measured free-space laser signal intensity over a 2.33 km optical path // Opt. Exp. 2007. V. 15. № 7. P. 3619–3628.

22. *Zamek S., Yitzhaky Y.* Turbulence strength estimation from an arbitrary set of atmospherically degraded images // J. Opt. Soc. America A. 2006. V. 23. № 12. P. 3106–3113.

23. *Gupta S.K., Mathew S.K., and Venkatakrishnan P.* Development of solar scintillometer // J. Astrophysics. 2006. V. 27. P. 315–320.

24. *Andrews L.C., Phillips R.L., and Hopen C.Y.* Laser beam scintillation with applications // Proc. SPIE, USA. 2001.

25. *Raj A.B., Selvi J.A.V., Kumar D., and Sivakumaran N.* Mitigation of beam fluctuation due to atmospheric turbulence and prediction of control quality using intelligent decision-making tools // Appl. Opt. 2014. V. 53. № 15. P. 3796–3806.

26. *Smith S.T.* MATLAB Advanced GUI Development. USA: Dog Ear Publishing, 2006.

27. *Font C.O., Chang M.P.J.L., Oh E., and Gilbreath C.* Humidity contribution to the refractive index structure function C_n^2 // SPIE Conf. "Atmospheric Propagation III". Florida, 2006. Part 6215. P. 1–9.